Clock and Power-Induced Bias Correction for UWB Time-of-Flight Measurements

Justin Cano, Gaël Pagès, Eric Chaumette, Jerome Le Ny

Clock and Power-Induced Bias Correction for UWB Time-of-Flight Measurements

Justin Cano, *Graduate Student Member, IEEE*, Gaël Pagès, *Member, IEEE*, Éric Chaumette, *Member, IEEE*, and Jérôme LeNy, *Senior Member, IEEE*

***Abstract*—Ultra-Wide Band (UWB) communication systems can be used to design low cost, power efficient and precise navigation systems for mobile robots, by measuring the Time of Flight (ToF) of messages traveling between on-board UWB transceivers to infer their locations. Theoretically, decimeter level positioning accuracy or better should be achievable, at least in benign propagation environments where Line-of-Sight (LoS) between the transceivers can be maintained. Yet, in practice, even in such favorable conditions, one often observes significant systematic errors (bias) in the ToF measurements, depending for example on the hardware configuration and relative poses between robots. This letter proposes a ToF error model that includes a standard transceiver clock offset term and an additional term that varies with the received signal power (RxP). We show experimentally that, after fine correction of the clock offset term using clock skew measurements available on modern UWB hardware, much of the remaining pose dependent error in LoS measurements can be captured by the (appropriately defined) RxP-dependent term. This leads us to propose a simple bias compensation scheme that only requires on-board measurements (clock skew and RxP) to remove most of the observed bias in LoS ToF measurements and reliably achieve cm-level ranging accuracy. Because the calibrated ToF bias model does not depend on any extrinsic information such as receiver distances or poses, it can be applied before any additional error correction scheme that requires more information about the robots and their environment.**

***Index Terms*—Range sensing, localization.**

I. Introduction

MOBILE robots require accurate position estimates in real-time to operate. Satellite Navigation Systems provide relatively reliable localization but only when the line-of-sight (LoS) between the receiver and sufficiently many satellites can be maintained. Hence, indoor and covered environments require alternative positioning systems, e.g., using machine vision or short-range radio-frequency (RF) communications [1]. This paper focuses on the latter, more specifically on Ultra-Wide Band (UWB) systems (see Fig. 1), which can provide low-cost, low-power, high-accuracy RF-based localization solutions for mobile robots, with a precision of the order of a decimeter in favorable conditions [2]–[10] and a refresh rate of the order of 10 to 100 Hz [11].

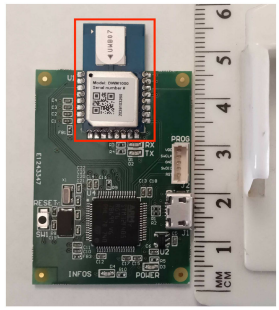

Fig. 1. Custom communication board used in our experiments. The UWB transceiver itself (Decawave DWM1000) and its omnidirectional antenna are encircled in red.

RF-based localization protocols most commonly rely on estimating the Time-of-Flight (ToF) of messages exchanged between transceivers, by comparing the transmission (Tx) and reception (Rx) times of these messages. ToF measurements can then be converted to distance measurements or used to synchronize some of the nodes [2], [11]. By design, UWB systems are relatively resilient to common sources of errors in ToF measurements [2]. Nonetheless, large positive errors can occur in non line-of-sight (NLoS) configurations, when the direct path between transceivers is blocked by an obstacle and the receiver detects instead a reflected signal. As a result, much of the literature on UWB-based localization focuses on detecting and mitigating the effect of NLoS measurements, see, e.g., [3], [12]–[14].

However, even in LoS conditions, ToF measurements are subject to errors due to transceiver clock drift, antenna delays, signal distortion, multipath interference and timestamp triggering uncertainties by the electronic circuits [5]. The Rx timestamp accuracy is particularly dependent on signal distortion and deteriorates as the received power (RxP) of the direct path signal

Manuscript received September 9, 2021; accepted January 10, 2022. Date of publication January 14, 2022; date of current version January 28, 2022. This letter was recommended for publication by Associate Editor D. Schulz and Editor S. Behnke upon evaluation of the reviewers' comments. This work was supported by FRQNT under Grant 2018-PR-253646. *(Corresponding author: Justin Cano.)*

Justin Cano is with the Department of Electrical Engineering, Polytechnique Montréal and with GERAD, Montréal H3T 1J4, QC, Canada, and also with the DEOS, ISAE-Supaéro, 31055 Toulouse, France (e-mail: justin.cano@polymtl.ca).

Gaël Pagès and Éric Chaumette are with the DEOS, ISAE-Supaéro, 31055 Toulouse, France (e-mail: gael.pages@isae-supaero.fr; eric.chaumette@isae.fr).

Jérôme LeNy is with the Department of Electrical Engineering, Polytechnique Montréal and with GERAD, Montréal H3T 1J4, QC, Canada (e-mail: jerome.le-ny@polymtl.ca).

This letter has supplementary downloadable material available at https://doi.org/10.1109/LRA.2022.3143202, provided by the authors.

Digital Object Identifier 10.1109/LRA.2022.3143202

decreases [5, p. 10]. These errors should be taken into account for accurate localization, since an offset of just one nanosecond in ToF estimation results in a ranging error of almost thirty centimeters, which is about the maximum tolerable for many indoor operations.

In practice, the systematic errors (bias) in UWB measurements need to be captured by empirical models that are sufficiently simple to be used in real-time positioning algorithms. González *et al.* [3] fit a model of two-way ranging (TWR) measurement bias in terms of distance between the transceivers, while [15] and [16] also include the relative antenna orientations in their models, for TWR and time-difference of arrival (TDoA) localization schemes respectively. Unfortunately, such models depend on extrinsic rather than intrinsic measurements, which are in fact often precisely what the higher-level localization schemes aim to estimate. For instance, distance pseudo-measurements are deduced from ToF measurements in various ways depending on the ranging protocol used at the application level (type of TWR scheme, TDoA, Time-of-Arrival (ToA), etc.) and full relative pose measurements between transceivers require additional sensors. Hence, any error in the distance or pose estimation scheme is fed back in the low-level measurement calibration, and these bias models are highly dependent on the specific localization scheme used. These models also do not take advantage of all the information available at the physical layer, in particular the channel impulse response (CIR) at the receiver, as well as the relative clock frequency drift measurements. Because the Rx timestamp is estimated from the CIR, errors can be fundamentally tied to it. Moreover, since the CIR and in particular the RxP is highly dependent on the antenna radiation pattern, it is quite plausible that most of the observed pose dependent bias can be already explained by the CIR features. Calibration models based on CIR features should also be less sensitive to system design choices such as level of transmitted power or type of antenna used, and to environmental characteristics such multipath propagation.

In this paper, we introduce a simple UWB ToF bias model for LoS measurements, capturing transceiver clock offset and RxP-induced bias, together with a methodology to calibrate such a model.

The application note [5] mentions a dependency of ToF measurement errors on RxP, but proposes again to calibrate ranging bias models (specifically for TWR) that are based indirectly on distance rather than CIR measurements, as in [3] for example. Savic *et al.* [17] propose a general model for TOA ranging measurements that includes a bias term for LoS measurements, but this term is constant (independent of the channel parameters) and the paper focuses on NLoS error mitigation. Wymeersch *et al.* [18] introduce machine learning-based methods to predict the ranging bias in TWR from the full CIR and a distance estimate, without distinguishing between LoS and NLoS measurements. As we discuss in Section III, their TWR calibration process can benefit from a preliminary clock skew correction step leveraging information available on more recent hardware. Compared to these papers, we focus exclusively on LoS measurements and develop a lightweight model linking ToF measurement bias to a type of RxP measurements. This model does not require extrinsic information such as relative transceiver poses, nor the full CIR but only its samples that are directly used in practice to determine the Rx timestamp. In a TWR localization experiment, we show that this model can capture most of the observed ranging bias. Moreover, this ToF bias model can be used with any type of localization scheme, e.g., TWR, TDoA, or ToA.

The outline of the paper is as follows. Section II introduces the ToF error model. Section III proposes a TWR-based clock offset correction scheme, which allows us to isolate the remaining RxP-induced bias in ToF measurements. This RxP-induced bias is modeled in more details in Section IV, which also introduces a methodology to calibrate it. Finally, Section V demonstrates in a TWR experiment that most of the bias in LoS measurements is captured by the model, and discusses further applications.

II. Time-of-Flight Measurement Model

Ideally, an UWB transmitter A and receiver B could measure the ToF τ_{AB} of a signal traveling in a direct path between them (LoS conditions) by taking the difference between the message reception time t_R and transmission time t_T, i.e., $\tau_{AB} = t_R - t_T$. This would provide for example a distance measurement $d_{AB} = c\,\tau_{AB}$ between the nodes, with c denoting the speed of light. However, a first difficulty is that each node measures time slightly differently according to its own imperfect clock. Second, even if the nodes were perfectly synchronized, timestamp measurements at each node are imperfect.

As mentioned previously, a dominating factor for the accuracy of t_R measurements is the received signal power (RxP) at B, $\mathcal{P}_R^B$. Indeed, the statistical performance of the algorithm estimating t_R, called the *Leading Edge Detector* (LDE), is known to be dependent on the received *Signal to Noise Ratio* (SNR) [5], [19]. As a result, we can model the timestamp measurement at the receiver as

$$t_R^B \approx t_R + \delta_c^B(t_R) + \delta_p^B(\mathcal{P}_R^B),$$

where $\delta_c^B(t_R)$ captures the clock offset of node B at absolute time t_R and δ_p^B is the RxP-dependent error. The timestamp measurement t_T^A at the transmitter follows the simpler model

$$t_T^A \approx t_T + \delta_c^A(t_T).$$

Taking the difference, we obtain the following ToF measurement model

$$t_R^B - t_T^A = \tau_{AB} + \delta_c^B(t_R) - \delta_c^A(t_T) + \delta_p^B(\mathcal{P}_R^B) + \nu, \quad (1)$$

where ν is a residual unmodeled error. For example, ν could include additional timestamp measurement errors due to imperfect calibration of antenna propagation delays.

For short-range communication systems such as those relying on UWB, the difference between t_R and t_T is of the order of the microsecond at most (which corresponds to a distance between nodes of about 300 m). This duration is too small for the offset δ_c of even low-grade electronic clocks to vary significantly. As a result, it is generally appropriate for short-range systems to use the simplified model

$$t_R^B - t_T^A = \tau_{AB} + \Delta_c^{B/A}(t_{R,T}) + \delta_p^B(\mathcal{P}_R^B) + \nu, \quad (2)$$

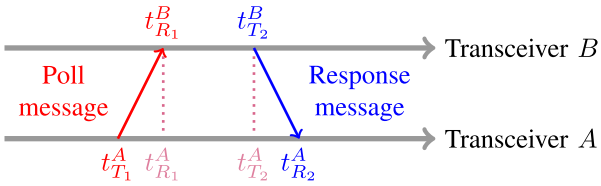

Fig. 2. Single-Sided TWR protocol.

where one can take for example $t_{R,T} = (t_T + t_R)/2$ and $\Delta_c^{B/A}(t)$ represents the offset of the clock of B with respect to the clock of A at time t. Then, to obtain accurate ToF measurements from the model (2) in practice, it is necessary to remove this clock offset as well as the RxP-induced error $\delta_p^B(\mathcal{P}_R^B)$. These topics are discussed in Sections III and IV respectively.

III. Clock Offset Correction: The Case of TWR

Clock offset correction is a well studied topic and is strongly dependent on the localization scheme. Hence, our discussion is short and focuses for concreteness on one of the simplest ranging scheme, single-sided TWR (SSTWR), see Fig. 2.

A SSTWR transaction involves two transceivers A and B. A transmits at time t_{T_1} a message to B, which is received at time t_{R_1}. B responds at t_{T_2} and this message is received at A at time t_{R_2}. We assume that the duration of the transaction is sufficiently short (of the order of a millisecond) to neglect the relative motion of the nodes. The TWR protocol tries to reduce the clock-offset error without synchronizing the nodes, by performing the following operation

$$\begin{aligned}&(t^B_{R_1} - t^A_{T_1}) + (t^A_{R_2} - t^B_{T_2})\\ &= 2\tau_{AB} + \Delta_c^{B/A}(t_1) - \Delta_c^{B/A}(t_2) + \delta_p^B(\mathcal{P}_R^B) + \delta_p^A(\mathcal{P}_R^A) + \nu,\end{aligned}$$

where ν is another residual error term and $t_1 \approx (t_{T_1} + t_{R_1})/2$, $t_2 \approx (t_{T_2} + t_{R_2})/2$. From this expression, we can approximate the ToF τ_{AB} by $\hat{\tau}_{AB}$ with

$$\hat{\tau}_{AB} = \tilde{\tau}_{AB} + \frac{\Delta_c^{B/A}(t_2) - \Delta_c^{B/A}(t_1)}{2} - \frac{\delta_p^B(\mathcal{P}_R^B) + \delta_p^A(\mathcal{P}_R^A)}{2}. \tag{3}$$

where $\tilde{\tau}_{AB} := \frac{t^B_{R_1} - t^A_{T_1} + t^A_{R_2} - t^B_{T_2}}{2}$.

Although standard versions of TWR approximate τ_{AB} by the first term and neglect in particular the difference $r_c^{B/A} := (\Delta_c^{B/A}(t_2) - \Delta_c^{B/A}(t_1))/2$ between clock offsets at the first and second messages, this term is often too large for accurate indoor navigation. To illustrate the impact of $r_c^{B/A}$, if we assume a constant typical clock skew of $\gamma := \partial\Delta_c^{B/A}/\partial t = 10^{-6}$ and a transaction time of $t_2 - t_1 = 2$ ms, we obtain $r_c^{B/A} = 1$ ns, which, as we noted before, would correspond to a ranging error of about 30 cm.

To correct this error, as explained in [11], we can leverage clock skew measurements $\tilde{\gamma}(t)$ already computed by the receiver of an UWB signal, which are recorded in the register set of current transceivers [20, p.150]. Indeed, the receiver needs to track the transmitter's oscillator frequency through a process called *timing recovery* [21, p.38], [22] in order to estimate the reception time of an UWB message with the correlation-based LDE algorithm. However, the measured clock skew $\tilde{\gamma}(t)$ is a noisy signal, which needs to be filtered to produce a more reliable estimate $\hat{\gamma}(t)$. The estimated clock skew $\hat{\gamma}$ can then be used to build an estimate of the residual clock error during a given transaction, as follows

$$\hat{r}_c^{B/A} = \frac{1}{2}\int_{t_1}^{t_2} \hat{\gamma}(\tau)d\tau \approx \frac{t_2 - t_1}{2}\hat{\gamma}, \tag{4}$$

where $\hat{\gamma}$ is the clock-skew estimate computed at time $t^A_{R_2}$ by agent A, with its own skew measurement $\tilde{\gamma}(t^A_{R_2})$.

The clock skew estimate $\hat{\gamma}$ can be updated at each SSTWR transaction k. Let's denote t_k the timestamp $t^A_{R_2}$ of transaction k. To filter $\tilde{\gamma}(t_k)$ and produce $\hat{\gamma}(t_k)$, we adapt our approach in [11] and use a Kalman filter with the following clock skew model

$$\begin{cases}\dot{\gamma} = \zeta_\gamma,\\ \tilde{\gamma}(t_k) = \gamma(t_k) + \nu_\gamma,\end{cases} \tag{5}$$

where ζ_γ is a centered Gaussian white noise with power spectral density $\sigma^2_{\gamma\gamma}$ and ν_γ a discrete centered Gaussian random variable with covariance $\sigma^2_{\gamma m}$. The constants $\sigma_{\gamma\gamma}$, $\sigma_{\gamma m}$ are tuned as explained in [11].

IV. RxP-Induced Error Correction

In this section, we present a methodology to estimate and correct the RxP-induced term $\delta_p^i(\mathcal{P}_R^i)$ in the ToF measurement model (1) or (2). This methodology requires selecting appropriate RxP measurements $\mathcal{P}_R$ at the receiver and then fitting the function $\delta_p^i(\mathcal{P}_R)$.

A. Most Informative RxP Measurements

The UWB transceivers used in our experiments (Decawave's `DW1000`) directly record two measures of received power in their register set [20], as follows. Let $\mathfrak{s}(t_i) = r(t_i) + jq(t_i) \in \mathbb{C}$ be the complex-valued CIR sampled at times t_i, $1 \le i \le N$, by an UWB module receiving a message. The *Average Received Power* (ARP) is defined as

$$\mathcal{P}_a = 10\log_{10}\left(\frac{1}{N^2}\sum_{i=1}^{N}|\mathfrak{s}(t_i)|^2\right) - \mathcal{P}_{ra},$$

with $\mathcal{P}_{ra}$ a reference power level. In constrast, the *First Path Power* (FPP) is defined as

$$\mathcal{P}_f = 10\log_{10}\left(\frac{1}{3^2}\sum_{i\in\mathcal{L}}|\mathfrak{s}(t_i)|^2\right) - \mathcal{P}_{rf},$$

where $\mathcal{P}_{rf}$ is another reference power level and $\mathcal{L} = \{i_1, i_2, i_3\}$ is a set of three characteristic amplitudes used by the LDE algorithm to determine the reception time of the message [20, p.40].

Our experiments lead us to choose the FPP instead of the ARP as a measure of received power to calibrate the function δ_p, since we found a clearer correlation between bias and $\mathcal{P}_f$ compared

to $\mathcal{P}_a$. One intuitive explanation is that $\mathcal{P}_f$ is directly used in the LDE algorithm and hence strongly affects its estimates. Moreover, $\mathcal{P}_a$ is more sensitive to disturbances due to multipath propagation, making the calibrated error model less robust to environmental changes. In practice, we noticed that the behavior of the FPP measured by transceivers in LoS and sufficiently far (beyond $50\,\mathrm{cm}$) from reflective surfaces (walls, ground, etc.) is repeatable at different locations. Hence, in the following we identify $\mathcal{P}_f$ as measure of RxP.

B. RxP-Induced Error Estimation Method

Based on our experimental results, we *postulate* for a given receiver i an RxP-induced error term of the form

$$\delta_p^i(\mathcal{P}_R^i) = K^i + \delta_p(\mathcal{P}_R^i), \tag{6}$$

where K^i is a receiver specific constant and the function δ_p is independent of i. In other words, the RxP-induced error for each UWB receiver (following a particular hardware design) is simply a shifted version of the function δ_p to determine. The constant K^i can be due to fabrication process variations for example.

In this section, we explain how to estimate the function δ_p. This can be done by taking ToF measurements between two transceivers A and B at various level of RxP, provided we can remove first the clock offset error $\Delta_c^{B/A}$ in (2). To do so, we can rely on the SSTWR scheme of Section III. From (3), we see that after estimating the residual clock error $\hat{r}_c^{B/A}$ from (4), we get

$$\frac{\delta_p^A(\mathcal{P}_R^A) + \delta_p^B(\mathcal{P}_R^B)}{2} \approx \tilde{\tau}_{AB} - \frac{d_{AB}}{c} + \hat{r}_c^{B/A}.$$

If we can assume $\mathcal{P}_R^A \approx \mathcal{P}_R^B = \mathcal{P}_R$ during the TWR exchange, then we obtain from (6)

$$\delta_p^{A,B}(\mathcal{P}_R) := \delta_p(\mathcal{P}_R) + K^{AB} \approx \tilde{\tau}_{AB} - \frac{d_{AB}}{c} + \hat{r}_c^{B/A}, \tag{7}$$

where $K^{AB} = \frac{K^A + K^B}{2}$ is an unknown constant depending on the pair (A, B) of transceivers. The assumption of approximately equal RxP at A and B during the SSTWR transaction is reasonable as long as we use omnidirectional antennas and the same transmitted power at A and B.

To estimate δ_p (up to a constant) based on (7), we can move a receiver A to different locations in an environment equipped with a precise external localization system, while maintaining LOS with a transmitter B at a fixed location. The goal is to sample sufficiently many values of RxP, covering the range of power values expected in subsequent deployment. At each position of A, the two transceivers perform multiple SSTWR transactions and we record all the quantities on the right-hand side of (7), including the distance d_{AB} measured by external localization. This provides bias measurements $\tilde{\delta}_p$ for the left-hand side of (7). We also collect RxP values $\tilde{\mathcal{P}}_R$ in each transaction, by reading the FPP recorded at the transceivers. FPP values $\tilde{\mathcal{P}}_f$ are recorded in dB but we found the logarithmic scale inconvenient to fit δ_p, so we perform a simple transformation and fit the function δ_p with $\tilde{\mathcal{P}}_R = 10^{(\tilde{\mathcal{P}}_f - \alpha_{\mathrm{dB}})/10}$ for some normalization parameter α_{dB} ($\alpha_{\mathrm{dB}} = -82\,\mathrm{dB}$ in our experiments). Since $\tilde{\mathcal{P}}_R^A \approx \tilde{\mathcal{P}}_R^B$ is only approximately true in general during a TWR transaction, we record the average RxP $\tilde{\mathcal{P}}_R = (\tilde{\mathcal{P}}_R^A + \tilde{\mathcal{P}}_R^B)/2$.

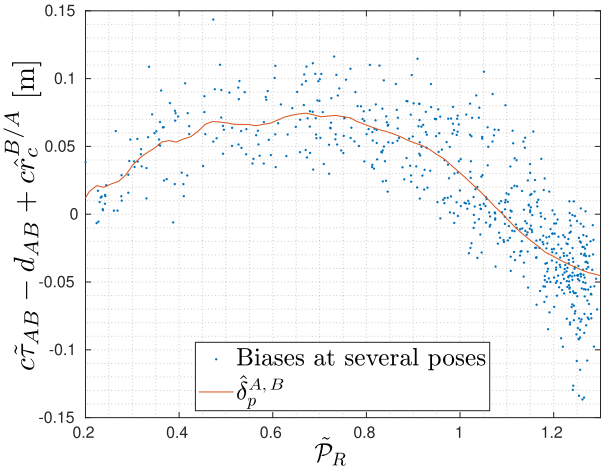

Fig. 3. An example of computed calibration map and RxP/bias data taken at several poses in the Polytechnique Montreal laboratory.

The resulting calibration dataset contains a large number of pairs $(\tilde{P}_R, \tilde{\delta}_p)$, one for each TWR transaction. To fit δ_p (up to the constant K^{AB}), we quantize the RxP into L values $\{\mathcal{P}_{R,i}\}_{i=1}^L$ uniformly spread between the minimum and maximum values observed for $\tilde{\mathcal{P}}_R$. The RxP-induced offset $\delta_p(\mathcal{P}_{R,i})$ for a given level $\mathcal{P}_{R,i}$ on the discretized grid is estimated by taking the empirical average of the observed bias $\tilde{\delta}_p$ for all corresponding RxP measurements $\tilde{\mathcal{P}}_R$ that are quantized to $\mathcal{P}_{R,i}$. We then store in a lookup table the L bias values $\{\delta_p(\mathcal{P}_{R,i})\}_{i=1}^L$ and compute any other value $\delta_p(\mathcal{P}_R)$ by linear interpolation. Fig. 3 shows an example of calibration dataset and fitted bias model.

For one-way ranging protocols (ToA, TDoA), the identification of the receiver dependent constant K^i in (6) is generally not needed, see Section VI. For TWR, the constant K^{AB} in (7) for a given pair of transceivers can be obtained by a short initialization phase, once δ_p is known. For this, we separate the transceivers by a known distance and let them perform a few SSTWR transactions. We then correct the ToF measurement for $\delta_p(\mathcal{P}_R)$ and $\hat{r}_c^{B/A}$, so that the remaining systematic bias in the measurements can be used to estimate K^{AB} from (7).

C. Experimental Validation

To validate the modeling assumptions and methodology presented in the previous section, in particular (7), we performed experiments at two different laboratories, in Montreal, Canada and Toulouse, France. FPP and RxP-induced bias measurements $(\tilde{P}_R, \tilde{\delta}_p)$ were obtained through SSTWR transactions with clock skew correction as described above, in multiple experiments with a fixed UWB transceiver B (anchor) and a mobile one A (tag) carried by an omnidirectional ground robot, see Fig. 4. Each laboratory is equipped with a motion capture system, providing the required distance measurements d_{AB} with mm-level accuracy.

The mobile node moved to different locations in the environment as illustrated on Fig. 4 and performed at each location a

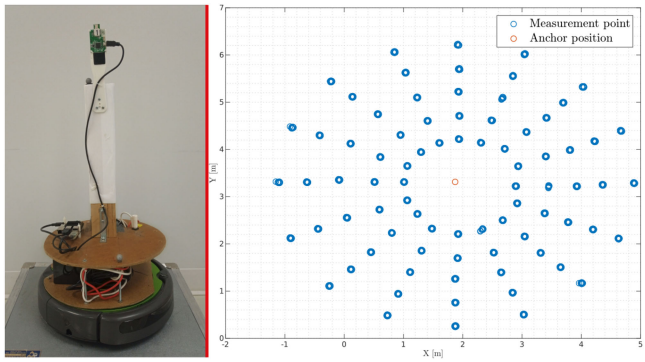

Fig. 4. Left: Robot used for our experiments. Right: Sampled positions of the tag around the anchor.

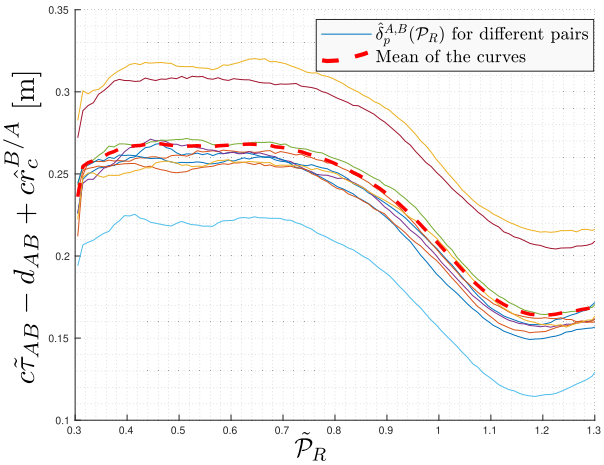

Fig. 5. Calibration maps for various pairs of modules (acquired at the ISAE laboratory in Toulouse).

full rotation to sample 8 different headings $\theta = k\pi/4, k \in [0, 7]$. The robot stops for 0.5 s at each pose to perform SSTWR with a refresh rate of 100 Hz. Therefore, we obtain about 50 measurements in each pose. Overall, this allows us to observe a sufficiently diverse set of RxP values. The data is recorded by an onboard computer running ROS and the function δ_p is fitted in a post-processing step after the complete dataset is collected. The results shown on Fig. 3 were obtained during one such experiment in Montreal.

Fig. 5 shows calibration curves $c\,\delta_p^{A,B}(\mathcal{P}_R)$ (see (7)) obtained by fitting the datasets of measurements $(\tilde{\mathcal{P}}_R, \tilde{\delta}_p)$ for ten different pairs (A, B) of UWB transceivers similar to the one shown on Fig. 1. These experiments were carried out in Toulouse and we used $L = 100$ quantization levels for the RxP. We observe that the curves indeed have a similar profile and mainly differ by their offset, i.e., they satisfy the model anticipated in (7). We noticed that the offset K^{AB} appears to be constant over time. We also plotted on Fig. 5 the calibration curve averaged over the previous 10 pairs of transceivers. This curve can serve as function δ_p to calibrate new pairs $(A,' B')$ of similar transceivers performing TWR transactions, which only requires estimating the offset $K^{A'B'}$, as explained at the end of Section IV-B.

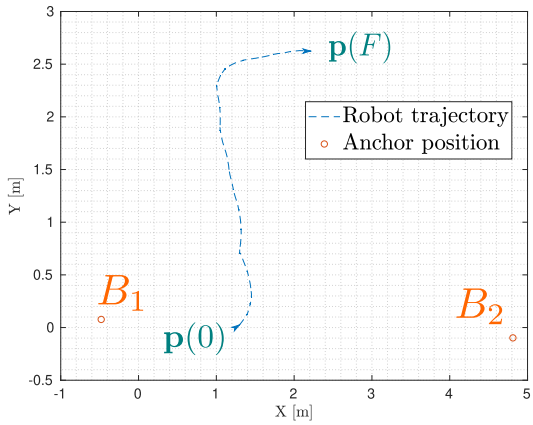

Fig. 6. Executed trajectory for the TWR localization test.

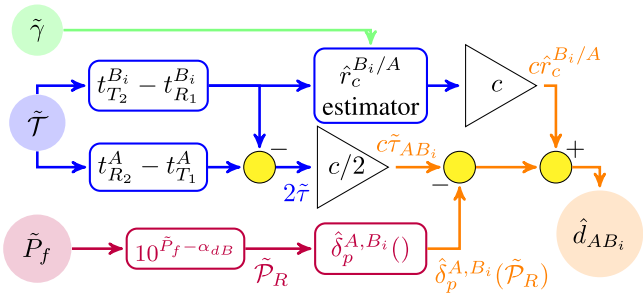

Fig. 7. Block diagram of the bias correction algorithm for each pair of transceivers A, B_i.

Figs 3 and 5 show that the calibration curves acquired in Toulouse and Montreal have a similar shape. This indicates that the estimated function $\delta_p^{AB}(\tilde{\mathcal{P}}_R)$ can be used to remove RxP-induced bias in LOS conditions in different environments. Indeed, the localization experiment presented in Section V has been repeated with calibration curves obtained in the other laboratory, which still provide a significant bias reduction. The main differences in the two sets of curves are observable at low RxP ($\tilde{\mathcal{P}}_R < 0.4$), where some environments more sensitive to multipath outliers degrade the accuracy of the calibration curves, and close to saturation ($\tilde{\mathcal{P}}_R > 1.2$). The latter differences could be explained by the fact that we used two different versions of the UWB modules (DWM1000) at the two locations, which may differ in their amplifier circuits and antennas.

V. TWR Localization Experiment

To evaluate the usefulness of performing a correction for clock skew and RxP-induced error, we carried out a localization experiment in 2D with a mobile UWB tag (playing the role of transceiver A in Fig. 2) performing SSTWR with two fixed UWB anchors B_1 and B_2 at known locations, see Fig. 6. The block diagram of the ranging algorithm implemented at the tag is shown on Fig. 7. The inputs of this algorithm are the measured timestamps $\tilde{\mathcal{T}} := \{t_{T_1}^A, t_{R_1}^{B_i}, t_{T_2}^{B_i}, t_{R_2}^A\}$, the clock skew measurements $\tilde{\gamma}$ and RxP $\tilde{\mathcal{P}}_R$ (derived from FPP measurements $\tilde{P}_f$). Note that all these inputs are directly provided by the UWB

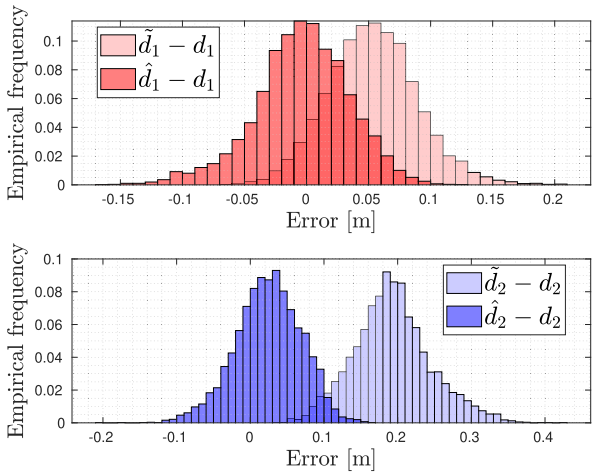

Fig. 8. Error histograms after and before compensation (calibrated with Montreal dataset).

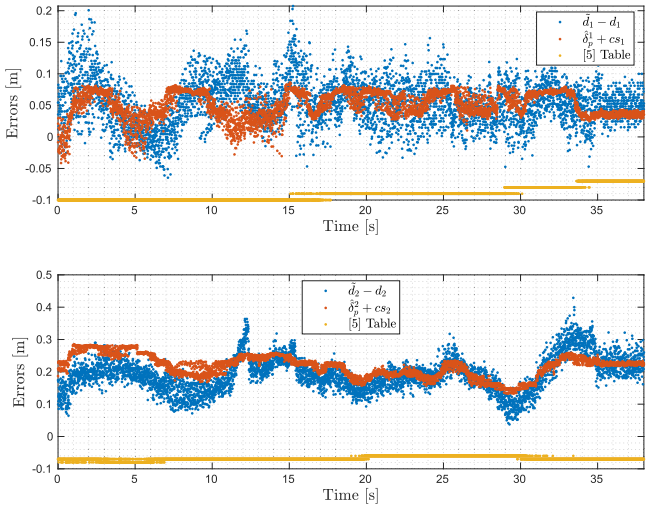

Fig. 9. Plot of raw range errors (blue), biases estimated by our method (orange) and biases predicted by the lookup table of [5] (yellow).

transceivers (the anchors can send their timestamps to the tag in their messages). The estimated range $\hat{d}_{AB}$ is obtained by elementary operations: i) time-related processing (in blue) consists of scalar elementary operations and a single state Kalman filter (estimator $\hat{r}_c^{B/A}$); ii) power-related processing (in purple) performs a simple linear interpolation using a lookup table containing just 100 RxP-induced bias values. The bias model δ_p used by the algorithm is the one previously estimated independently from the dataset presented in Section IV-C. The initialization phase described at the end of Section IV-B is performed for each pair (anchor, tag) in order to estimate the constants K^{AB}. The algorithm can provide corrected range estimates between the tag and anchors with an update frequency of 100 Hz.

Fig. 6 shows the two anchors at coordinates $\mathbf{B}_1 = [-0.48, 0.08, 1.69]^\top$ and $\mathbf{B}_2 = [4.81, -0.10, 1.69]^\top$ and the trajectory of the mobile tag from the initial position $\mathbf{p}(0)$ to the final position $\mathbf{p}(F)$. This trajectory, measured by the motion capture system, is produced by the *D-Opt* motion planner presented in [23], which aims to compute positions that reduce the ranging-based localization error for the robot. We denote d_i the true distance between the anchor B_i and the tag, measured by the motion capture system. The raw UWB range measurements between the tag and anchor $i \in \{1, 2\}$ are denoted $\tilde{d}_i = c\,\tilde{\tau}_{AB_i}$, while $\hat{d}_i$ are the corrected range estimates produced by the algorithm of Fig. 7.

Fig. 8 shows the histograms of error values for raw and corrected UWB range measurements. The time series of these experiments, presenting raw errors and biases estimated by the algorithm, are plotted in Fig. 9. The apparent offset at the beginning of the trajectory might be due to the time it takes for the clock offset estimate $\hat{r}_c^{B/A}$ to converge. Note that large range measurement outliers, presumably due to reflected signals, where removed from the dataset, since we focus on LoS conditions. Overall, the corrected range measurements present a residual bias below two centimeters, while this bias was typically close to $20\,\mathrm{cm}$ for the range to anchor 2 before correction.

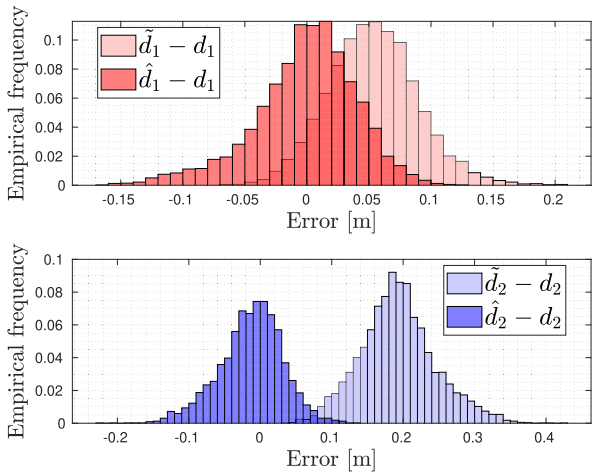

Fig. 10. Error histograms after and before compensation (calibrated with Toulouse dataset).

Since the residual noise after bias correction shows a standard deviation of 3 to 5 cm, we see that it is crucial for accurate range measurements to correct the bias error. Fig. 9 also provides a comparison with the bias predicted by the lookup table of the application note [5, Table 1] (our implementation sets the PRF to 64 MHz and uses channel 2). This table attempts to correct the bias based on the uncorrected distance estimates obtained from TWR, but it clearly fails here to track the bias, possibly because of the significant differences in hardware.

We repeated the calibration process for the experiment presented on Fig. 6, which took place in Montreal, using the mean calibration map acquired in Toulouse, plotted on Fig. 5. The accuracy of the bias correction, illustrated in Fig. 10, slightly deteriorated compared to that of Fig. 8, but the average ranging error remained below $3\,\mathrm{cm}$ for both anchors. Finally, in a video accompanying this article, we illustrate the calibration process

and the validation on the previously presented trajectory with dynamic plots.

VI. Application to Other Localization Schemes

In this section, we briefly discuss how the ToF model (2) with RxP-induced bias model (6) is useful to correct errors in different RF-based localization schemes, such as ToA and TDoA [1]. Both ToA and TDoA systems require multiple *synchronized* UWB anchors $A_1, \dots, A_M$ placed at known locations $\mathbf{p}_{A_i}$ and broadcasting localization messages, while any number of UWB-equipped tags can determine their location by listening to these messages.

Consider a tag B receiving a message from anchor A_i. For ToA, we can write from (2) and (6)

$$\begin{aligned}\rho_i &:= c(t^B_{R_i} - t^{A_i}_{T_i}) \\ &\approx d_{A_iB} + c\Delta^{B/A}_c + c\delta^B_p(\mathcal{P}^B_{R,i}) \\ &\approx d_{A_iB} + D + c\delta_p(\mathcal{P}^B_{R,i}),\end{aligned} \tag{8}$$

where $D = \Delta^{B/A}_c + K^B$ is independent of the index i of anchor A_i because the anchors are synchronized (and we neglect here the time variation of the clock offset $\Delta^{B/A}_c$) and K^B only depends on the receiver B. To determine its position, the tag records the M pseudo-range measurements ρ_i and corresponding FPP values $\mathcal{P}_{R,i}$ to solve the least-squares problem

$$\min_{\mathbf{p},D} \sum_{i=1}^{M} \left|\rho_i - \|\mathbf{p} - \mathbf{p}_{A_i}\| - c\delta_p(\mathcal{P}^B_{R,i}) - D\right|^2. \tag{9}$$

A well-posed problem requires at least $M = d + 1$ anchors for localization in d dimensions. A minimizer $(\mathbf{p}, D)$ of (9) produces an estimate $\mathbf{p}_B$ of the position of B and an estimate of the constant D, which is discarded. Hence, we see that the constant K^B does not need to be calibrated separately, the knowledge of the function δ_p is enough to correct the RxP-induced error in ToA.

Similarly, for TDoA, a tag B receiving messages from two anchors A_i and A_j computes the double difference

$$\begin{aligned}\Delta_{ij} &:= c(t^B_{R_i} - t^{A_i}_{T_i}) - c(t^B_{R_j} - t^{A_j}_{T_j}) \\ &\approx d_{A_iB} - d_{A_jB} + c(\delta_p(\mathcal{P}^B_{R,i}) - \delta_p(\mathcal{P}^B_{R,j})).\end{aligned}$$

The clock offsets cancel out because the anchors are synchronized (and we neglect the offset time variations). So does the constant K^B, which does not depend on the anchor. To determine its position, tag B records the Δ_{ij} for all pairs of anchors, as well as the FPP $\mathcal{P}^B_{R,i}$ for all messages. It then solves the least-squares problem

$$\begin{aligned}\min_{\mathbf{p}} \sum_{i\neq j} \Big|\Delta_{ij} - \|\mathbf{p} - \mathbf{p}_{A_i}\| + \|\mathbf{p} - \mathbf{p}_{A_j}\| \\ - c\delta_p(\mathcal{P}^B_{R,i}) + c\delta_p(\mathcal{P}^B_{R,j})\Big|^2.\end{aligned} \tag{10}$$

Again, correction of RxP-induced errors for TDoA depends only on identifying the function δ_p and not the constant K^B.

VII. Conclusion

We developed an empirical bias model for UWB ToF measurements in LoS conditions. The input variable of the model is the received power (RxP), which can be measured directly by UWB receivers from the channel impulse response. We proposed a methodology based on a TWR protocol to calibrate the RxP-induced bias model, which leverages relative clock skew measurements available on current receivers to first correct residual clock offsets. We verified empirically that the identified bias model is relatively robust to changing environmental conditions and that it can be used to significantly improve localization accuracy in practice. An important advantage of the bias correction method is that it does not require external measurements nor a complex model that depends on estimating the robot or environment parameters. If more is known about those parameters, additional corrections could be applied as a second step, for example to identify NLoS measurements. Future work will apply the bias correction method to other localization protocols and consider more complex signal propagation scenarios.

Acknowledgment

The authors would like to thank Corentin Chauffaut and Louis Treton from ISAE for their availability and their assistance.

References

[1] P. D. Groves, *Principles of GNSS, Inertial, and Multisensor Integrated Navigation Systems*, 2nd ed. Boston, USA: Artech House, 2013.

[2] Z. Sahinoglu, S. Gezici, and I. Guvenc, *Ultra-Wideband Positioning Systems: Theoretical Limits, Ranging Algorithms, and Protocols*. Cambridge, UK.: Cambridge Univ. Press, 2008.

[3] J. González *et al.*, "Mobile robot localization based on ultra-wide-band ranging: A particle filter approach," *Robot. Auton. Syst.*, vol. 57, no. 5, pp. 496–507, 2009.

[4] Amanda Prorok, "Models and algorithms for ultra-wideband localization in single- and multi-robot systems," Ph.D. dissertation, École Polytechnique Fédérale de Lausanne, Switzerland: Lausanne, 2013.

[5] *Decawave*, "Sources of error in DW1000 based TWR schemes," Qorvo, Tech. Rep. APS011, 2018. [Online]. Available: https://www.decawave.com/wp-content/uploads/2018/10/APS011_Sources-of-Error-in-Two-Way-Ranging-Schemes_v1.1.pdf

[6] A. Ledergerber and R. D' Andrea, "Ultra-wideband range measurement model with Gaussian processes," in *Proc. IEEE Conf. Control Technol. Appl.*, 2017, pp. 1929–1934.

[7] M. Hamer and R. D'Andrea, "Self-calibrating ultra-wideband network supporting multi-robot localization," *IEEE Access*, vol. 6, pp. 22 292–22 304, 2018.

[8] V. Mai *et al.*, "Local positioning system using UWB range measurements for an unmanned blimp," *IEEE Robot. Automat. Lett.*, vol. 3, no. 4, pp. 2971–2978, Oct. 2018.

[9] A. D. Preter, G. Goysens, J. Anthonis, J. Swevers, and G. Pipeleers, "Range bias modeling and autocalibration of an UWB positioning system," in *Proc. Int. Conf. Indoor Positioning Indoor Navigation*, 2019, pp. 1–8.

[10] B. Van Herbruggen *et al.*, "Wi-PoS: A low-cost, open source ultra-wideband (UWB) hardware platform with long range sub-GHz backbone," *Sensors*, vol. 19, no. 7, Jan. 2019, Art. no. 1548.

[11] J. Cano, S. Chidami, and J. Le Ny, "A Kalman filter-based algorithm for simultaneous time synchronization and localization in UWB networks," in *Proc. Int. Conf. Robot. Automat.*, Montreal, QC, Canada, 2019, pp. 1431–1437.

[12] S. Marano, W. M. Gifford, H. Wymeersch, and M. Z. Win, "NLOS identification and mitigation for localization based on UWB experimental data," *IEEE J. Sel. Areas Commun.*, vol. 28, no. 7, pp. 1026–1035, Sep. 2010.

[13] K. Bregar and M. Mohorčič, "Improving indoor localization using convolutional neural networks on computationally restricted devices," *IEEE Access*, vol. 6, pp. 17 429–17 441, 2018.
[14] J. Zhu and S. S. Kia, "Bias compensation for UWB ranging for pedestrian geolocation applications," *IEEE Sens. Lett.*, vol. 3, no. 9, pp. 1–4, Sep. 2019.
[15] A. Ledergerber and R. D'andrea, "Calibrating away inaccuracies in ultra wideband range measurements: A maximum likelihood approach," *IEEE Access*, vol. 6, pp. 78 719–78 730, 2018.
[16] W. Zhao, J. Panerati, and A. P. Schoellig, "Learning-based bias correction for time difference of arrival ultra-wideband localization of resource-constrained mobile robots," *IEEE Robot. Automat. Lett.*, vol. 6, no. 2, pp. 3639–3646, Apr. 2021.
[17] V. Savic, E. G. Larsson, J. Ferrer-Coll, and P. Stenumgaard, "Kernel methods for accurate UWB-based ranging with reduced complexity," *IEEE Trans. Wireless Commun.*, vol. 15, no. 3, pp. 1783–1793, Mar. 2016.
[18] H. Wymeersch, S. Marano, W. M. Gifford, and M. Z. Win, "A machine learning approach to ranging error mitigation for UWB localization," *IEEE Trans. Commun.*, vol. 60, no. 6, pp. 1719–1728, Jun. 2012.
[19] I. Sharp, K. Yu, and Y. J. Guo, "Peak and leading edge detection for time-of-arrival estimation in band-limited positioning systems," *IET Commun.*, vol. 3, no. 10, pp. 1616–1627, 2009.
[20] *Decawave*, "DW1000 user manual, V2.18," 2017. [Online]. Available: https://www.decawave.com/dw1000/usermanual/
[21] K. Aldubaikhy, "Differential code-shifted reference impulse-radio ultra-wideband receiver: Timing recovery and digital implementation," *Master's Thesis*, Dalhousie Univ., 2012. [Online]. Available: http://dalspace.library.dal.ca/handle/10222/15244
[22] K.-B. Png, X. Peng, S. Chattong, H. T. Francis, and F. Chin, "Joint carrier and sampling frequency offset estimation for MB-OFDM UWB system," in *Proc. IEEE Radio Wireless Symp.*, 2008, pp. 29–32.
[23] J. L. Ny and S. Chauvière, "Localizability-constrained deployment of mobile robotic networks with noisy range measurements," in *Proc. Amer. Control Conf.*, 2018, pp. 2788–2793.